Int. J. Heat Mass Transfer. Vol. 28, No. 12, pp. 2353–2361, 1985
Printed in Great Britain

0017–9310/85 $3.00 + 0.00

Heat transfer at the base of a cylindrical cavity oriented perpendicular to a freestream flow

E. M. SPARROW and G. T. GEIGER
Department of Mechanical Engineering, University of Minnesota, Minneapolis, MN 55455, U.S.A.

(*Received* 17 *May* 1985 *and in final form* 22 *July* 1985)

Abstract—The average and local heat transfer at the base surface of a cylindrical cavity whose opening is perpendicular to an oncoming freestream have been determined experimentally. During the course of the experiments, the cavity depth was varied from zero to 65% of the diameter, while the freestream Reynolds number ranged between about 5000 and 50,000. The average heat transfer coefficient decreased sharply with increasing cavity depth, the reduction being slightly greater than 50% at a depth–diameter ratio of 0.10 and greater than 90% when the depth–diameter ratio was 0.65. For the finite-depth cavities, the local heat transfer coefficient attained its maximum value at the center of the base surface and decreased with increasing radial distance from the center until a minimum was reached, after which there was a moderate increase adjacent to the outer edge of the base. The minimum occurred at the location where the radial outflow along the base separated from the surface, and a toroidal-shaped recirculation zone occupied the corner region at the intersection of the cavity base and side wall. In contrast, for the zero-depth cavity (i.e. a free disk oriented perpendicular to the oncoming flow), the local coefficient attained its minimum at the center of the surface and increased with increasing radial distance from the center.

INTRODUCTION

THIS PAPER is concerned with the heat transfer from cavities which is induced by a forced convection flow external to the cavity opening. The previous work on this subject has dealt almost exclusively with problems where the external flow is parallel to the plane of the opening. Here, consideration is given to the other fundamental case of cavity/external flow interaction—the case in which the external flow is perpendicular to the cavity opening.

The response of the cavity heat transfer to the two parameters on which it depends was investigated experimentally. The experiments were performed with cylindrical cavities and air as the participating fluid, with the parameters being the Reynolds number of the freestream flow and the cavity depth–diameter ratio. The Reynolds number was varied by an order of magnitude between about 5000 and 50,000, while the cavity depth ranged between zero and 65% of the diameter.

The experiments yielded two types of results. One of these is the average heat transfer coefficient, while the other is the radial distribution of the local heat transfer coefficient on the base surface of the cavity. The average coefficients are of more direct use in practice, but the local coefficients provide insights into the patterns of fluid flow in the cavity. Both the average and the local results for the various cavity depths will be compared with the corresponding results for the cavity of zero depth.

The accuracy of the results was enhanced by the use of the naphthalene sublimation technique, whereby heat transfer results are obtained from mass transfer measurements. In the present application, this technique offers the advantages of negligible extraneous losses, well-defined and well-controlled boundary conditions, high local resolution, high measurement accuracy, and apparatus simplicity and flexibility. Independent measurements were made to determine the local coefficients and the average coefficients.

It appears that the only prior investigation of heat transfer for flow perpendicular to the opening of the cylindrical cavity is that of ref. [1], which was performed as a parachute simulation. Because of the measurement technique, the heat transfer results may be more qualitative than quantitative. Relevant aspects of [1] will be discussed during the presentation of results.

EXPERIMENTAL APPARATUS AND PROCEDURE

Apparatus

A schematic pictorial diagram of the test-section portion of the experimental apparatus is presented in Fig. 1. As seen there, a cylindrical sleeve of inside diameter D houses a naphthalene disk (also of diameter

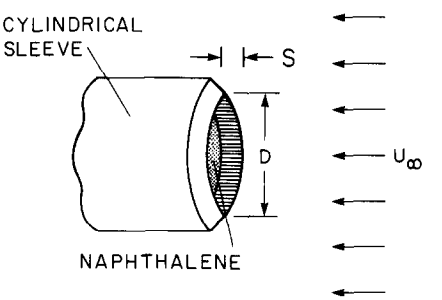

FIG. 1. Schematic of the cylindrical cavity used in the experiments.

NOMENCLATURE

A	area of base surface
D	diameter of base surface
$\mathscr{D}$	diffusion coefficient
$K(r)$	local mass transfer coefficient, equation (3)
K_0	value of $K(r)$ at center of base
$\bar{K}$	average mass transfer coefficient, equation (1)
ΔM	change of mass during data run
$\dot{m}(r)$	local mass flux
$\overline{Nu}$	average Nusselt number
Pr	Prandtl number
R	radius of base surface
Re	freestream Reynolds number, $U_\infty D/\nu$
r	radial coordinate
S	cavity depth
Sc	Schmidt number
$Sh(r)$	local Sherwood number, $K(r)D/\mathscr{D}$
Sh_0	value of $Sh(r)$ at center of base
$\overline{Sh}$	average Sherwood number, $\bar{K}D/\mathscr{D}$
U_∞	freestream velocity.

Greek symbols

$\delta(r)$	local surface recession
δ_0	value of $\delta(r)$ at center of base
ν	kinematic viscosity
ρ_{nw}	naphthalene vapor density at surface
$\rho_{n\infty}$	naphthalene vapor density in freestream
ρ_s	density of solid naphthalene
τ	duration of data run.

Other symbol

[ ]*	zero-depth cavity.

D) whose surface is situated at a distance S from the open end of the sleeve. The disk forms the base surface of a cylindrical cavity, while the exposed inside surface of the sleeve forms the side wall of the cavity. The cavity geometry is defined by the depth–diameter ratio S/D.

The naphthalene disk is the front face of a short aluminum cylinder which fits snugly in the bore of the sleeve. Hereafter, the cylinder–disk assembly will be referred to as the centerbody of the test section. The centerbody can be moved axially within the bore of the sleeve in order to set the cavity depth S, which, once set, is locked in place. At its rear face, the centerbody is coupled to a sting-like support rod which extends downstream in the axial direction.

The metallic portion of the centerbody was drilled along its axis to provide a passage for the pouring of molten naphthalene during the casting of the naphthalene disk. In addition, two smaller axial holes were provided to vent the air displaced during the casting process. Thermocouple leads were drawn through one of these holes, enabling a thermocouple junction to be cast into the exposed face of the naphthalene disk. The measured surface temperature facilitated the evaluation of the naphthalene vapor pressure adjacent to the surface.

To accommodate the naphthalene disk, a shallow (0.7-cm deep) recess was machined in the front face of the metallic portion of the centerbody. The outer wall of the recess was tapered to virtually zero thickness ($\sim$0.005 cm) at its forwardmost edge. Both the base and the wall of the recess were roughened to aid in the adhesion of the naphthalene.

The cylindrical sleeve is of brass, with an internal diameter of 3.500 cm and a wall thickness of 0.457 cm. At its forward edge, the sleeve was beveled at 45° in order to minimize the blockage of the flow due to the finite wall thickness of the sleeve. The axial length of the sleeve is 3.175 cm.

The support rod which mates with the downstream face of the centerbody is the forwardmost member of a system which serves both to support the test section and to position the cavity opening perpendicular to the oncoming freestream. The perpendicular positioning was facilitated by a universal joint attached to the downstream end of the support rod. In turn, the universal joint was rigidly supported by a stand which was bolted to the floor of the wind tunnel in which the experiments were performed. The crossflow members of the stand were sufficiently far downstream so that their presence did not affect the flow about the test section.

As a supplement to the test section, an impermeable cap was fabricated which, when put in place over the cavity opening, suppressed sublimation at the naphthalene surface. The cap was used during the preparatory stage of each data run, during which time the test section was allowed to attain thermal equilibrium with the airflow in the wind tunnel. It was also used when transporting the test section between the wind tunnel and the instrumentation laboratory where the mass transfer measurements were made.

Instrumentation

The determination of the average mass transfer coefficient requires data on the mass which sublimes from the entire transfer surface during a known period of time. This information is most accurately obtained by measuring the mass of the centerbody as a whole immediately before and immediately after a data run, and then differencing the measured masses. The mass measurements were made with a Sartorius ultra-precision analytical balance with a resolution of 10^{-5} g and a capacity of 166 g. (Note that the alternative procedure of averaging the local mass transfer distribution is, necessarily, less accurate than the adopted procedure.) During a typical data run, the

change of mass was in the 0.015–0.030 g range, which corresponds to a mean surface recession of 0.0005–0.001 in.

The local mass transfer coefficients were determined from the local sublimation-related recession of the naphthalene surface. To this end, the contour of the naphthalene surface was measured both before and after a data run. For the contour measurements, the centerbody was placed on a horizontal coordinate table so that its axis was vertical and the naphthalene surface faced upward. A fixture rigidly attached to the table served to precisely and reproducibly position the centerbody and to hold it in place. The coordinate table could be traversed in two perpendicular horizontal directions with an accuracy of 0.0025 cm or better.

The surface contours were measured by an electronic depth gage suspended from a fixed strut which overhung the coordinate table. The measurement system consisted of a stylus, a linear variable differential transformer, signal conditioning electronics, and a printer-equipped digital voltmeter. The system output was strictly linear and yielded 0.01 V per 0.001 in. of vertical displacement of the stylus, with the last digit of the printout corresponding to 10^{-5} in.

Static pressures, needed in the determination of the freestream velocity and the density of the airflow, were measured using a solid-state, capacitance-type pressure meter capable of resolving 10^{-3} Torr.

Wind tunnel

The experiments were performed in a suction-type wind tunnel operated in the open-circuit mode. Room air, pre-mixed to ensure temperature uniformity, was drawn through a set of screens and a 20 : 1 contraction into the working section of the wind tunnel, from which it passed successively through an axial fan and a diffuser, finally being discharged outside the building. The outside discharge ensured that the room air (and, therefore, the freestream flow in the working section) was free of naphthalene vapor.

The cross section of the tunnel working section was a 30.48 × 60.96 cm rectangle (height × width), with a 2.44 m streamwise length. The axis of the cavity was centered in the cross section, and the apparatus was positioned well away from both the inlet and outlet of the working section. Since the ratio of the cavity opening to the tunnel cross section was only 0.5%, blockage effects were negligible and no blockage corrections were made.

The freestream velocity U_∞ was measured by an impact tube and a wall static tap situated upstream and to the side of the cavity. The impact tube was traversed perpendicular to the tunnel wall to ensure that the freestream velocity was being measured well outside the wall boundary layer. For the present experiments, U_∞ ranged from about 2.1 to 21 m s^{-1}, which corresponds to a Reynolds number range from about 5000 to 50,000 (with the cavity opening as the characteristic dimension). In the velocity range of the experiments, the freestream turbulence level was 0.4–0.5%.

Experimental procedure

At the beginning of the experimental work, the cavity opening was carefully aligned to be perpendicular to the freestream, and the alignment was verified periodically during the course of the experiments. The alignment was accomplished by using the oil–lampblack flow visualization technique [2, pp. 53–56]. To this end, the cavity was set at zero depth, so that the naphthalene surface coincided with the cavity opening. The oil–lampblack mixture was then applied to the surface of a sheet of white, plasticized, self-adhering contact paper which covered the naphthalene.

When exposed to the airflow, the oil–lampblack mixture revealed both the stagnation point and the radial flow emanating from the stagnation point. With the aid of the universal joint, the orientation of the cavity opening was adjusted so that the stagnation point occurred precisely in the center of the opening and the radial lines exhibited perfect axisymmetry—indicating the attainment of perpendicular alignment. The setting of the universal joint corresponding to the aligned condition was quantified by means of protractor readings.

To prepare for a data run, the naphthalene disk from the prior run was removed from the centerbody by melting and evaporation and a new disk was cast in place. The surface finish of the exposed face of the naphthalene was comparable to that of the highly polished stainless steel plate against which it was cast.

Each data run was preceded by the measurement of the mass of the centerbody and, for selected runs, the contour of the naphthalene surface was measured. The surface traverses were made along four radial lines (i.e. two perpendicular diameters). Then, the test section, capped to prevent sublimation, was placed in the wind tunnel to attain thermal equilibrium. Once a steady state had been achieved, the protective cap was removed, thereby initiating the data run proper. During the data run, both the naphthalene surface temperature and the velocity pressure of the airflow were monitored and recorded. To terminate the run, the cavity opening was capped and the test section removed from the wind tunnel. The duration of the run was selected to limit the average recession of the naphthalene surface to 0.001 in. The run was immediately followed by mass and surface contour measurements.

To determine the extraneous mass transfer during the measurement and setup periods, all events which occurred between the pre-run and post-run measurements were repeated, except that the cavity was not exposed to the airflow. A correction was made for the thus-determined extraneous mass loss (about 2%).

RESULTS AND DISCUSSION

Data reduction

The average mass transfer coefficient $\bar{K}$ for the cavity base surface was determined from the sublimation-related change of mass ΔM, the duration τ of the data

run, the transfer surface area A, and the naphthalene vapor densities which drive the mass transfer. With these,

$$\bar{K} = \Delta M/\tau A(\rho_{nw} - \rho_{n\infty}) \quad (1)$$

in which ρ_{nw} is the vapor density at the subliming surface and $\rho_{n\infty}$ is the vapor density in the freestream. To determine ρ_{nw}, the measured naphthalene surface temperature was used as input to the vapor pressure/temperature relation for naphthalene [3] and, in turn, the vapor pressure and temperature were used to evaluate ρ_{nw} from the perfect gas law. The freestream is devoid of naphthalene vapor in the present experiments, so that $\rho_{n\infty} = 0$.

The dimensionless counterpart of the average mass transfer coefficient is the average Sherwood number $\overline{Sh}$ defined as

$$\overline{Sh} = \bar{K}D/\mathscr{D} \quad (2)$$

where $\mathscr{D}$, the mass diffusion coefficient, was evaluated from a formula given by Skelland [4, p. 51]. Furthermore, with $\mathscr{D}$ and with the kinematic viscosity ν (evaluated for pure air because of the minute concentrations of naphthalene vapor), the Schmidt number $Sc = \nu/\mathscr{D}$ was found to be 2.55 for all of the operating conditions of the experiments.

Attention will next be turned to the local mass transfer coefficient $K(r)$. If $\delta(r)$ denotes the local sublimation-related recession of the surface which occurs at a radial position r during a time interval τ, then the local rate of mass transfer $\dot{m}(r)$ per unit area is given by $\rho_s\delta/\tau$, where ρ_s is the density of solid naphthalene. Then,

$$K(r) = \dot{m}(r)/(\rho_{nw} - \rho_{n\infty}). \quad (3)$$

If K_0 denotes the local mass transfer coefficient at the center of the base surface (i.e. at $r = 0$), the ratio $K(r)/K_0$ reduces to

$$K(r)/K_0 = \delta(r)/\delta_0 \quad (4)$$

and, since $Sh(r) = K(r)D/\mathscr{D}$,

$$Sh(r)/Sh_0 = \delta(r)/\delta_0. \quad (5)$$

The local mass transfer results will be presented in terms of the Sherwood number ratio expressed by equation (5).

To determine $\delta(r)$ from the experimental data, the pre-run surface contours measured along four radial lines were averaged to yield a single radial distribution, and similarly for the post-run surface contours. The pre-run and post-run radial distributions were then differenced, yielding $\delta(r)$.

The fluid flow aspects of the problem were expressed in terms of the freestream Reynolds number

$$Re = U_\infty D/\nu. \quad (6)$$

Average Sherwood numbers

The experimental data for the average Sherwood number at the cavity base surface are presented in Fig. 2. In the figure, $\overline{Sh}$ is plotted as a function of the freestream Reynolds number Re for parametric values of the cavity depth–diameter ratio S/D equal to 0.10, 0.29, 0.47 and 0.65. The data for each cavity depth are interconnected by least-squares straight lines. To help provide perspective for the effect of the cavity depth, a solid line representing the average Sherwood number results for the zero-depth cavity [3, 5] has been included in the figure (the zero-depth cavity is actually a free disk oriented perpendicular to the freestream).

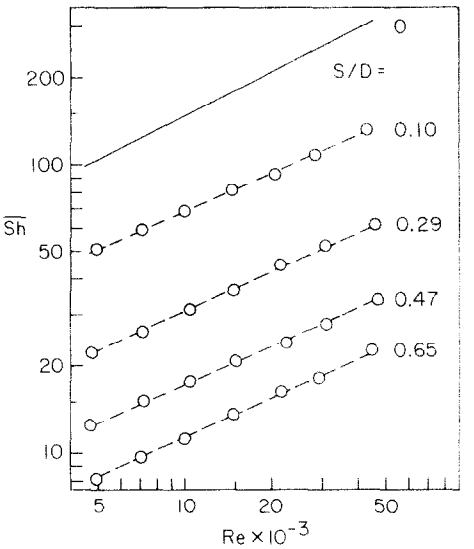

FIG. 2. Average base-surface Sherwood numbers.

Inspection of the figure shows that the base-surface Sherwood number is markedly affected by the cavity depth, decreasing sharply as the depth increases. Even for a very shallow cavity such as $S/D = 0.10$, the Sherwood numbers are about one-half of those for the zero-depth cavity. When the cavity depth is about half the diameter (by no means a very deep cavity), the Sherwood numbers are seen to be about one order of magnitude smaller than the zero-depth values. Further perspectives on the effect of cavity depth will be presented shortly.

The aforementioned low mass transfer coefficients suggest that very little of the freestream flow—a smaller and smaller portion with increasing cavity depth—is able to penetrate to the cavity base. This state of affairs was confirmed when the oil–lampblack technique was employed to visualize the flow along the base surface. Even for the most shallow of the investigated cavities ($S/D = 0.10$), the velocities adjacent to the base surface were too small to activate the oil–lampblack mixture (i.e. the least stiff mixture that would not sag under gravity).

Figure 2 also shows that for a given cavity depth, the dependence of $\overline{Sh}$ on Re is logarithmically linear, that is, $\overline{Sh} = C\,Re^n$. The slopes n, determined via least squares, were found to be virtually the same for the various cavity depths. The slight differences among the slopes were averaged out, yielding $n = 0.445$. The constants C,

determined to fit the representation

$$\overline{Sh} = C\,Re^{0.445} \quad (7)$$

were equal to 1.141, 0.517, 0.286 and 0.189 for $S/D = 0.10$, 0.29, 0.47 and 0.65, respectively. The extreme deviation of the data from equation (7), used in conjunction with the aforementioned C values, is about 3%.

The Reynolds-number dependence of the cavity-base Sherwood number is slightly different from that for the zero-depth cavity. For the latter, from [3] and [5],

$$\overline{Sh} = 1.47\,Re^{1/2}. \quad (8)$$

The difference in the Reynolds-number dependence is due to the different patterns of fluid flow, as will be elucidated when the local Sherwood numbers are presented.

To highlight the effects of cavity depth, the data of Fig. 2 have been cross-plotted so that the depth–diameter ratio S/D plays the role of the independent variable. In the resulting figure, Fig. 3, $\overline{Sh}$ vs S/D variations are presented for three representative Reynolds numbers, 5000, 15,000 and 40,000. The figure shows that the sharpest dropoff of $\overline{Sh}$ occurs at small cavity depths and that the dropoff becomes somewhat more gradual as the depth increases. For sufficiently deep cavities, the Sherwood number should approach zero. Of particular note in Fig. 3 is the fact that the slopes of the curves for the three Reynolds numbers are virtually identical, indicating that in the investigated range, the response of $\overline{Sh}$ to changes in S/D is nearly independent of the Reynolds number.

It is informative to make a direct comparison of the Sherwood numbers at the base of a finite-depth cavity with those for a cavity of zero depth. If the average Sherwood numbers for the latter are denoted by $[\overline{Sh}]^*$, then the ratio $\overline{Sh}/[\overline{Sh}]^*$ embodies the desired direct comparison. This ratio is plotted against the Reynolds number in Fig. 4 for parametric values of S/D. As seen in the figure, $\overline{Sh}/[\overline{Sh}]^*$ depends only weakly on the Reynolds number. From equations (7) and (8), the dependence is $Re^{-0.055}$, which amounts to about 12% over the investigated order of magnitude in Re.

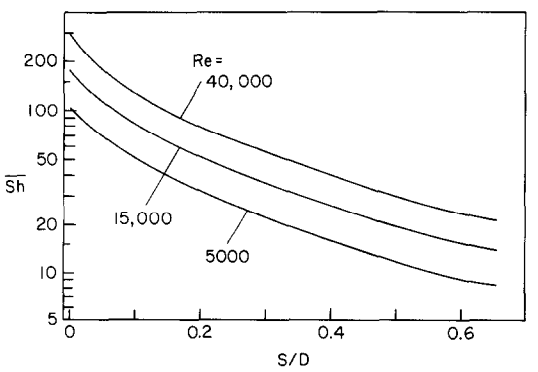

FIG. 3. Effect of cavity depth on the base-surface Sherwood number.

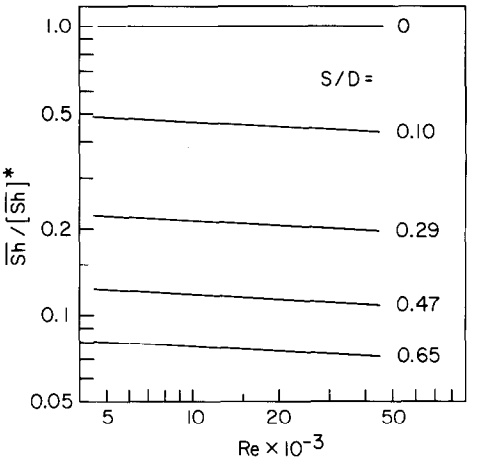

FIG. 4. Comparison of average base-surface Sherwood numbers for finite-depth cavities and zero-depth cavities.

The main message of Fig. 4 is the magnitude of $\overline{Sh}/[\overline{Sh}]^*$, the values of which for the respective S/D are approx. 0.45, 0.21, 0.11 and 0.075. These results suggest a means for reducing the forced convection heat transfer from a surface that is impinged by a perpendicular flow. This can be accomplished by creating cavities in the surface. According to Fig. 4, such cavities can be effective even when they are relatively shallow.

Local Sherwood number distributions

The radial distributions of the local Sherwood number $Sh(r)$ are presented in Figs. 5–7, respectively for cavity depths characterized by $S/D = 0.10$, 0.29 and 0.65. Each radial distribution is normalized by its own centerline value Sh_0, so that all distributions start with the value $Sh(r)/Sh_0 = 1$ at $r = 0$. The abscissa is the dimensionless radial coordinate r/R, which ranges from 0 to 1. For each cavity depth, results are presented for three representative Reynolds numbers, $Re = 7000$, 15,000 and 45,000, and the data for each Reynolds number are interconnected by smooth curves to provide continuity. These results are referred to the left-hand ordinate.

Also appearing in each figure is a dashed line, taken from [5], which represents the radial distribution of the local Sherwood number for the cavity of zero depth (i.e. a free disk oriented perpendicular to the freestream). As demonstrated in [5], $Sh(r)/Sh_0$ is virtually independent of the Reynolds number in the investigated range, so that the results can be conveyed by a single (dashed) line, common to all the figures. The dashed line is referred to the right-hand ordinate, where an asterisk has been appended to $Sh(r)/Sh_0$ to call attention to the fact that it pertains to the zero-depth cavity.

The differences between the radial distributions for the finite-depth cavities and the zero-depth cavity are so striking as to demand immediate discussion. These differences are reflected both in the shapes of the distributions and in the magnitudes of $Sh(r)/Sh_0$. For

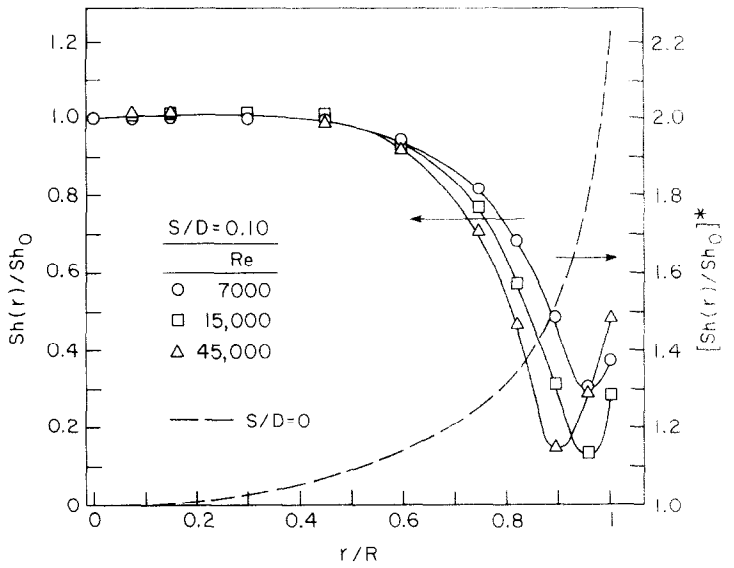

FIG. 5. Radial distributions of the local base-surface Sherwood number, $S/D = 0.10$.

the zero-depth cavity, $[Sh(r)/Sh_0]^*$ increases monotonically with radial position, gradually at first and then more and more rapidly, culminating in a virtually vertical rise at the outer edge of the surface. For all radial positions, $[Sh(r)/Sh_0]^*$ exceeds unity and attains a maximum value of approx. 2.2.

In contrast, for the finite-depth cavities, $Sh(r)/Sh_0$ decreases from its initial value of unity, and the decrease becomes more rapid with increasing radial position until, in the outer reaches of the surface, a reversal occurs—resulting in a minimum and a subsequent increase. In general, $Sh(r)/Sh_0$ is less than unity and attains values as low as 0.15 at the minimum.

The aforementioned differences in the local Sherwood number distributions reflect major differences in the pattern of fluid flow adjacent to the base surface. As already noted, for the zero-depth cavity, the base surface becomes a free disk, and the freestream flow impinging on the disk sets up a surface-adjacent radial outflow. At the outer edge of the disk, the radial flow turns sharply in the downstream direction, resulting in a pinching together of the streamlines in that region and a consequent rapid acceleration of the fluid. The thinning of the boundary layer associated with the turning and the acceleration is responsible for the rapid rise of $[Sh(r)]^*$ near the edge of the disk. The fact that $[Sh(r)]^*$ increases with r at all radial positions indicates that the boundary-layer thickness decreases

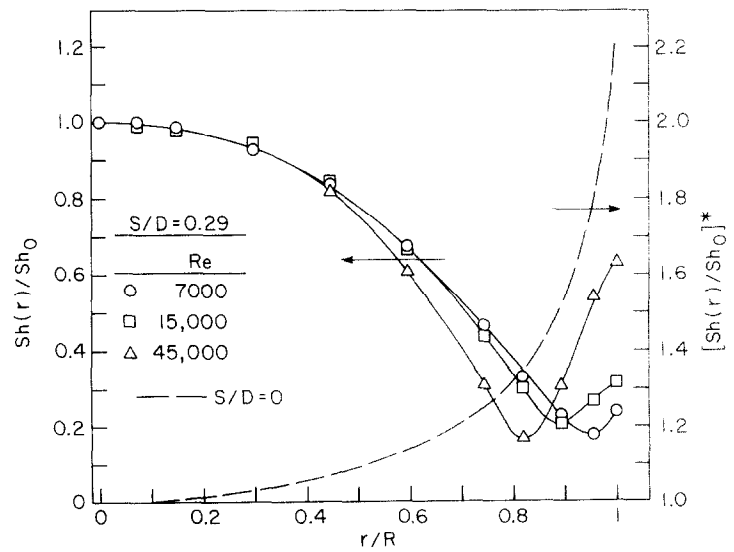

FIG. 6. Radial distributions of the local base-surface Sherwood number, $S/D = 0.29$.

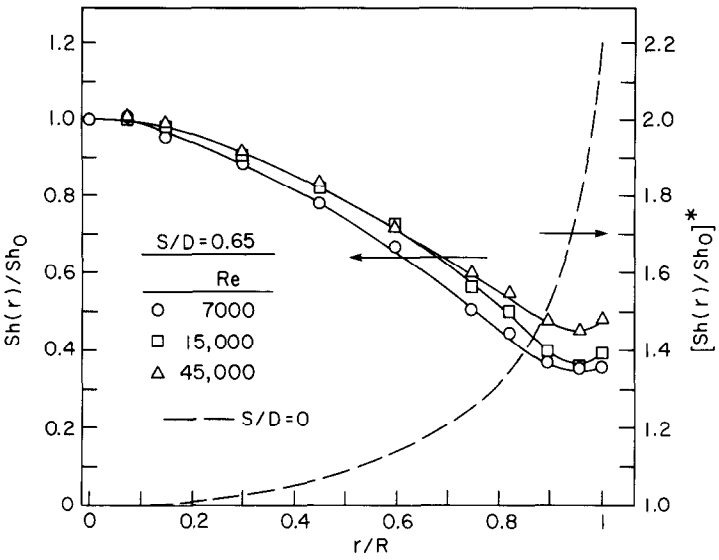

FIG. 7. Radial distributions of the local base-surface Sherwood number, $S/D = 0.65$.

with r over the entire disk, showing that the effects of the turning and the acceleration are felt all the way to the center of the disk.

The $Sh(r)$ distributions for the finite-depth cavities are also indicative of a radial outflow along the base surface—an outflow which, however, does not penetrate into the sharp corner at the intersection of the cavity base and side wall. Rather, before reaching the corner, the radial flow separates from (i.e. lifts off) the base surface. The corner region is occupied by a toroidal-shaped recirculation zone.

The decrease of $Sh(r)$ along the base surface indicates that the boundary layer embedded in the aforementioned radial outflow grows thicker with increasing r, and the minimum value of $Sh(r)$ corresponds to the location at which the boundary layer separates from the surface. The increase of $Sh(r)$ beyond the separation location is the result of the scrubbing action of the recirculating flow on the surface.

It is interesting to note that the $Sh(r)$ distributions of Figs. 5–7 are very similar in shape to the distribution of the local heat transfer coefficient around the circumference of a cylinder in crossflow [6, p. 343]. Furthermore, the foregoing rationalization of the shape of the distribution also applies for the latter case.

Further inspection of Figs. 5–7 reveals various features of the $Sh(r)$ distributions which testify to the lesser penetration of the freestream into the cavity as the depth increases. For increasing S/D, these factors include the shrinking of the region adjacent to $r = 0$ where $Sh(r)$ is relatively uniform, the more shallow minimum, and the lesser rebound of the Sherwood number after separation. These features respectively correspond to a more immediate boundary-layer growth in the radial outward flow, a substantially lower value of Sh_0 which gives rise to a larger value of $Sh(r)/Sh_0$ at separation, and a less vigorous recirculation in the corner region. All of these are symptoms of the reduced extent of the freestream flow which penetrates to the cavity base.

Discussion

The depth-related reductions in the average base-surface Sherwood number found here are greater than the reductions in the average Nusselt number set forth in [1]. In general, the deviation may be ascribed to the transient technique used in [1] (described there as being inherently inaccurate). In particular, the fact that the results of [1] are high can also be made plausible.

The apparatus used in [1] consisted, in essence, of a blunt-edged plexiglass sleeve and a bakelite centerbody. The sleeve–centerbody assembly was heated prior to the data run and, during the run, the temperature–time histories of five small aluminum plugs embedded in the centerbody were monitored and the local heat transfer coefficients determined therefrom.

Since bakelite is not a very good insulator ($k = 1.4$ W m^{-1} °C^{-1} [6]) and since the convective heat transfer coefficients at the base surface of a cavity are small, it is likely that the aluminum plugs exchanged heat by conduction with the bakelite as well as by convection with the airflow. The presence of the conduction may well have influenced the temperature–time histories at all of the plugs, but it is especially likely to have affected the outermost plug, which was situated in a region of particularly low heat transfer coefficients. At that plug, the conduction acted to increase the apparent rate of heat transfer and, therefore, the heat transfer coefficients obtained from the transient method were too high.

Average heat transfer coefficients were not measured directly in [1] but rather were computed by averaging

the local coefficients obtained at the five aforementioned embedded plugs. For the averaging, the local coefficient at the outermost plug was weighted by nearly 50% of the surface area of the cavity base. As already discussed, the local coefficient at the plug is believed to have been high due to conduction in the bakelite. These considerations make plausible the relatively high average Nusselt numbers presented in [1]. In addition, aside from the conduction issue, the local coefficient at the outermost plug ($r/R = 0.85$), even if it were perfectly accurate, was probably different than the proper value that is representative of the outermost area element used in the averaging.

CONCLUDING REMARKS

The Sherwood number results presented here can be transformed into Nusselt numbers by using the well-established analogy between heat and mass transfer. For example, for the average Sherwood and Nusselt numbers corresponding to a fixed Reynolds number,

$$\overline{Nu} = (Pr/Sc)^m \overline{Sh} \tag{9}$$

where the exponent m is usually taken as 1/3 for boundary-layer flows. The local Sherwood and Nusselt numbers are also related by an equation similar to (9).

The experimental results have provided definitive information about the heat/mass transfer at the base of a cylindrical cavity whose opening is aligned perpendicular to the oncoming freestream flow. The average Nusselt/Sherwood numbers were found to decrease sharply with increasing cavity depth. For a shallow cavity with a depth–diameter ratio of 0.10, the base-surface Nusselt/Sherwood numbers were less than half those for the zero-depth cavity (i.e. a free disk oriented perpendicular to the flow). For a cavity depth–diameter ratio of 0.65 (by no means a very deep cavity), the Nusselt/Sherwood numbers were only about 7.5% of the zero-depth values. The average base-surface Sherwood numbers were correlated to within 3% by equation (7) in conjunction with the appended coefficients, and the average Nusselt numbers follow from equation (9).

The radial distribution of the local Nusselt/Sherwood number along the base of the cavity exhibited drastically different shapes for the finite-depth and the zero-depth cavities. The latter distribution took on its minimum value at the center of the base and its maximum value at the outer edge, with a monotonic increase between. On the other hand, for the former, the maximum occurred at the center. The local Nusselt/Sherwood numbers decreased with increasing distance from the center, attained a minimum in the outer reaches of the base surface, and then increased toward the outer edge. This behavior corresponds to a radial outflow which separates from the base surface before it reaches the outer edge (i.e. the corner at which the base and the side wall meet). The corner region is occupied by a toroidal-shaped recirculation zone.

The results obtained here indicate that cavities can be used effectively to reduce the forced convection heat transfer from a surface that is impinged by a perpendicular flow. Significant reductions can be achieved even when the cavities are relatively shallow.

REFERENCES

1. J. C. Y. Koh and J. P. Hartnett, Pressure distribution and heat transfer for flow over simulated cylindrical parachutes, *J. Heat Transfer* **87**, 521–525 (1965).
2. W. Merzkirch, *Flow Visualization*. Academic Press, New York (1974).
3. H. H. Sogin, Sublimation from disks to air streams flowing normal to their surfaces, *Trans. Am. Soc. mech. Engrs* **80**, 61–71 (1958).
4. A. H. P. Skelland, *Diffusional Mass Transfer*. Wiley, New York (1974).
5. E. M. Sparrow and G. T. Geiger, Local and average heat transfer characteristics for a disk situated perpendicular to a uniform flow. *J. Heat Transfer* **107**, 321–326 (1985).
6. F. P. Incropera and D. P. DeWitt, *Fundamentals of Heat Transfer*. Wiley, New York (1981).

TRANSFERT THERMIQUE A LA BASE D'UNE CAVITE CYLINDRIQUE ORIENTEE PERPENDICULAIREMENT A UN ECOULEMENT LIBRE

Résumé—On détermine expérimentalement le transfert thermique moyen et local sur la surface de base d'une cavité cylindrique dont l'ouverture est perpendiculaire à un écoulement libre incident. Au cours d'expériences, la profondeur de la cavité varie de zéro à 65% du diamètre, tandis que le nombre de Reynolds de l'écoulement varie entre 5000 et 50 000. Le coefficient de transfert moyen diminue fortement quand la profondeur de cavité augmente, la réduction étant légèrement supérieure à 50% à un rapport profondeur-diamètre de 0, 10 et supérieure à 90% quand ce rapport est 0,65. Pour les cavités de profondeur finie, le coefficient de transfert local atteint son maximum au centre de la base et décroît quand augmente la distance radiale au centre de la base jusqu'à atteindre un minimum, puis un léger accroissement se fait près du bord extérieur de la base. Au contraire, pour la cavité de profondeur nulle (par exemple, un disque libre orienté perpendiculairement à l'écoulement incident), le coefficient local atteint son minimum au centre de la surface et augmente avec la distance radiale du centre.

WÄRMEÜBERGANG AM BODEN EINES ZYLINDRISCHEN HOHLRAUMES, DER SENKRECHT ZU EINER FREIEN STRÖMUNG STEHT

Zusammenfassung—Der mittlere und örtliche Wärmeübergang an dem Boden eines zylindrischen Hohlraums, dessen Öffnung senkrecht zur vorbeifließenden freien Strömung angeordnet ist, wurde experimentell untersucht. Bei den Experimenten wurde die Tiefe des Hohlraums von 0 auf 65% des Durchmessers verändert, die Reynolds-Zahl der freien Strömung lag zwischen 5000 und 50 000. Der mittlere Wärmeübergangskoeffizient nimmt mit zunehmender Tiefe des Hohlraums stark ab. Die Abnahme ist etwas größer als 50% bei einem Tiefen/Durchmesser-Verhältnis von 0,10 und größer als 90%, wenn das Tiefen/Durchmesser-Verhältnis 0,65 beträgt. Für Hohlräume mit endlicher Tiefe erreicht der örtliche Wärmeübergangskoeffizient seinen größten Wert im Mittelpunkt der Bodenfläche und nimmt bei größeren Radien ab, bis ein Minimum erreicht wird. Danach stellt man einen leichten Anstieg bis zum äußeren Rand des Bodens fest. Das Minimum tritt an der Stelle auf, wo sich die radiale Strömung entlang des Bodens von der Oberfläche ablöst. In der Ecke zwischen dem Boden und der Seitenwand tritt eine torusförmige Rezirkulationszone auf. Im Gegensatz dazu erreicht ein Hohlraum mit der Länge Null (das ist eine freie Scheibe, die senkrecht zur Strömung steht) das Minimum der örtlichen Wärmeübergangskoeffizienten im Mittelpunkt der Oberfläche. Mit zunehmendem Radius nimmt der örtliche Wärmeübergangskoeffizient zu.

ТЕПЛООБМЕН У ОСНОВАНИЯ ЦИЛИНДРИЧЕСКОЙ ПОЛОСТИ, РАСПОЛОЖЕННОЙ ПЕРПЕНДИКУЛЯРНО НАБЕГАЮЩЕМУ ПОТОКУ

Аннотация—Проведено экспериментальное определение средней и локальной плотности теплового потока на нижней поверхности цилиндрической полости, ориентированной открытой ее стороной перпендикулярно набегающему потоку. В экспериментах глубина полости изменялась от 0 до 65% величины ее диаметра, а значения числа Рейнольдса для набегающего потока изменялось в пределах 5000–50000. С увеличением глубины полости средний коэффициент теплообмена резко уменьшался, причем это уменьшение несколько превышало 50% при отношении глубины к диаметру, равном 0,1 и превышало 90%, когда отношение глубины к диаметру составляло 0,65. Для полостей конечной глубины локальный коэффициент теплообмена достигал своего максимума в центре поверхности основания и уменьшался с увеличением расстояния по радиусу от центра, достигая минимума, после которого начиналось умеренное его увеличение вблизи внешнего края основания. Минимум наблюдался в месте отрыва от поверхности основания радиального внешнего потока, а тороидальная зона рециркуляции располагалась в угловой области у пересечения основания с боковой цилиндрической поверхностью. Для полости с нулевой глубиной (т.е. для диска, расположенного перпендикулярно набегающему потоку) напротив, локальный коэффициент достигал своего минимума в центре поверхности основания и возрастал по мере увеличения расстояния по радиусу от центра.